Electronic Supplementary Material (ESI) for Inorganic Chemistry Frontiers.

Cotton textile inspires MoS_2@reduced graphene oxide anodes towards high-rate capability or long-cycle stability sodium/lithium-ion batteries

Xue Liu,[a,b‡]* Haicong Ji,[a‡] Bin Peng,[a] Zhaoning Cui,[a] Qiongzhen Liu,[a] Qinghua Zhao,[a] Liyan Yang[a] and Dong Wang[a,c]*

[a]*Key Laboratory of Textile Fiber and Products (Wuhan Textile University), Ministry of Education, Hubei International Scientific and Technological Cooperation Base of Intelligent Textile Materials & Application, College of Materials Science and Engineering, Wuhan Textile University, Wuhan 430200, China*

[b]*Key Laboratory of Advanced Energy Materials Chemistry (Ministry of Education), College of Chemistry, Nankai University, Tianjin 300071, China*

[c]*College of Chemistry, Chemical Engineering and Biotechnology, Donghua University, Shanghai, 201620, China*

***Corresponding author**

Email: xueliu@wtu.edu.cn; wangdon08@126.com

‡These authors contribute equally to this work

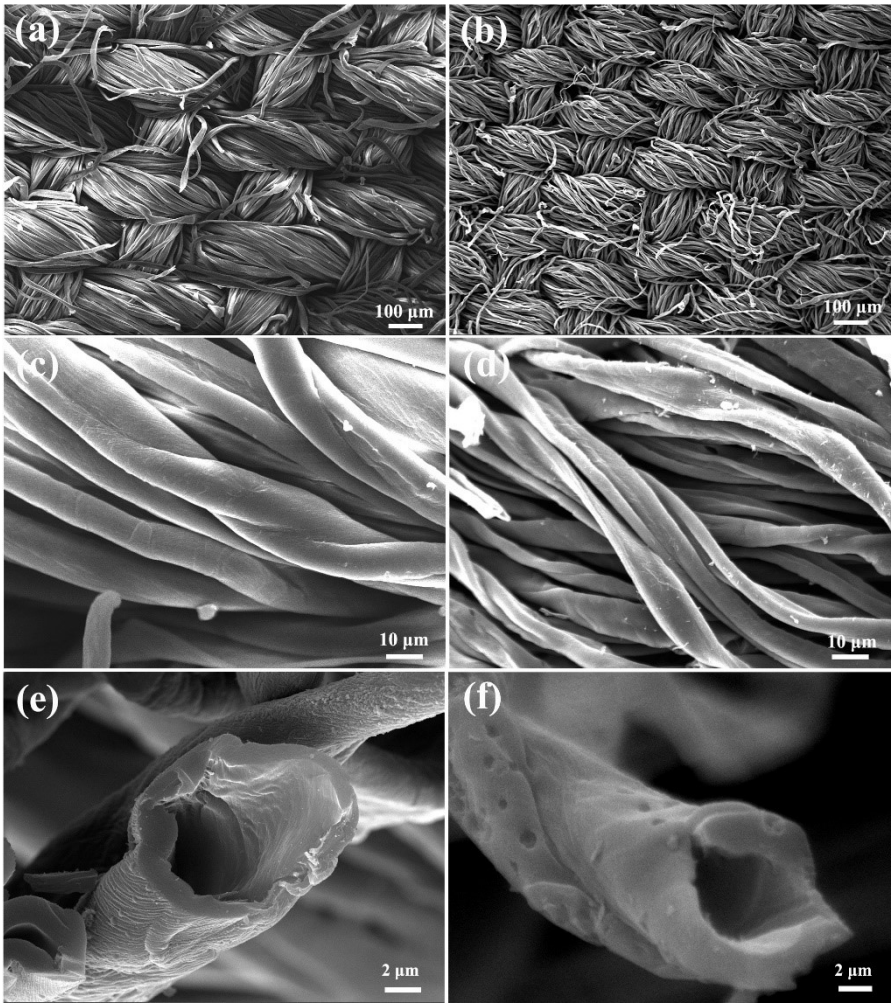

Figure S1. SEM images of cotton textile (a,c,e) before and (b,d,f) after annealing at 900 °C.

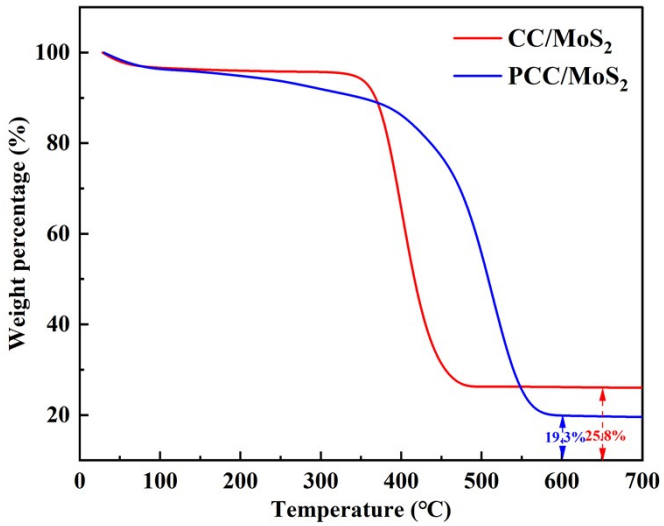

Figure S2. TGA curves of CC/MoS_2-1.5 and PCC/MoS_2-1.5.

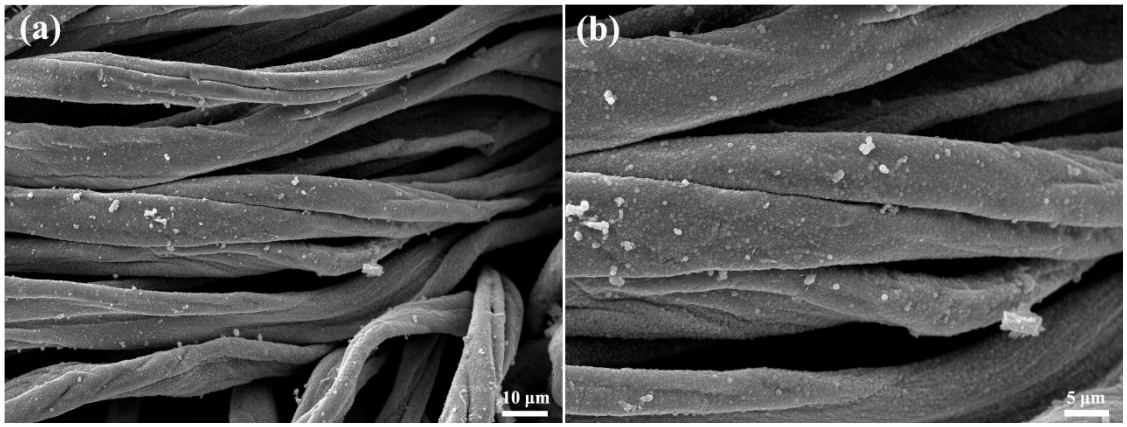

Figure S3. Low-magnification SEM images of CC/MoS_2-1.5.

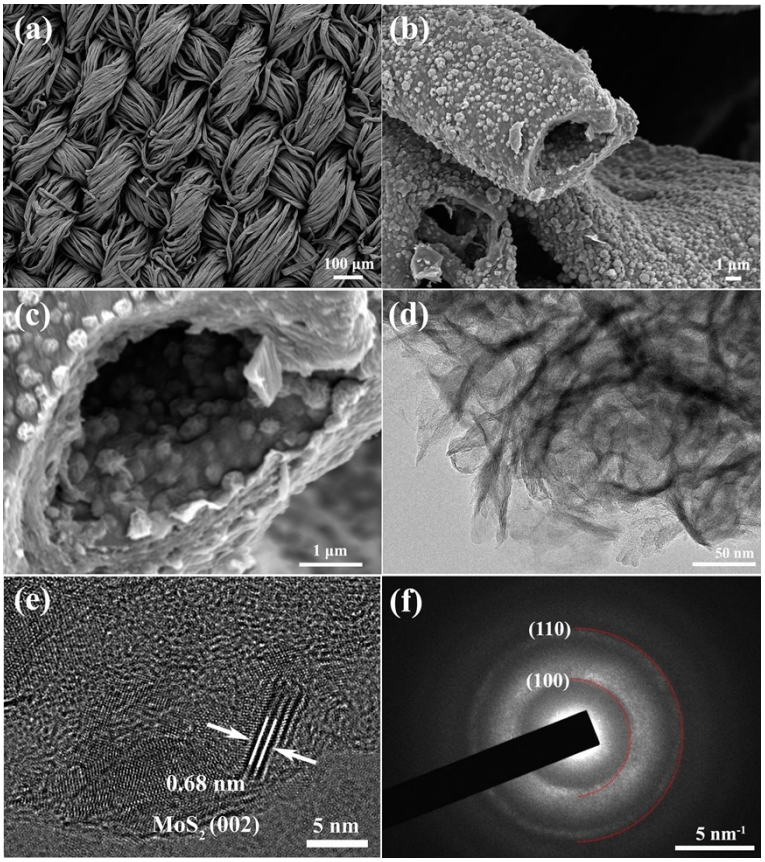

Figure S4. (a-c) SEM images of CC/MoS_2@RGO-700 textile at different magnifications. (d, e) TEM images of CC/MoS_2@RGO-700 textile. (f) The SAED pattern of CC/MoS_2@RGO-700 textile.

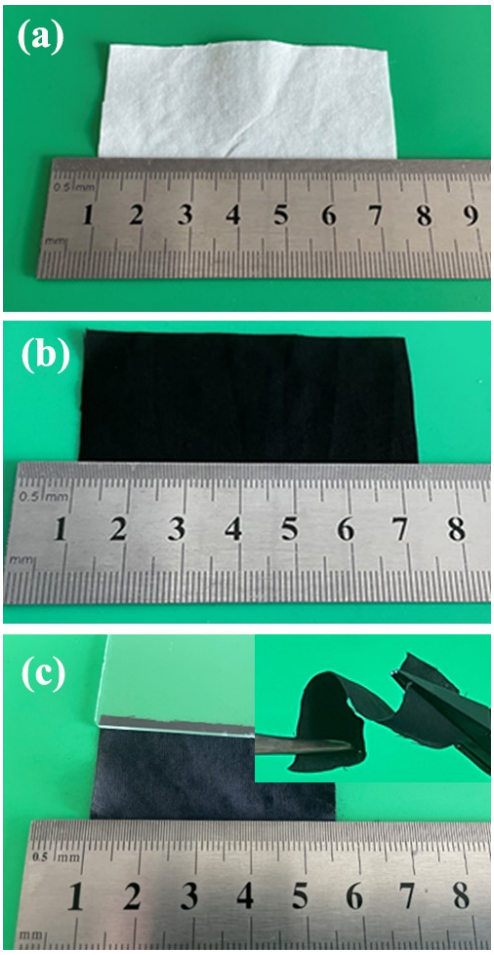

Figure S5. Digital images of (a) Cotton, (b) Cotton/MoS_2, and (c) CC/MoS_2@RGO-700 textile.

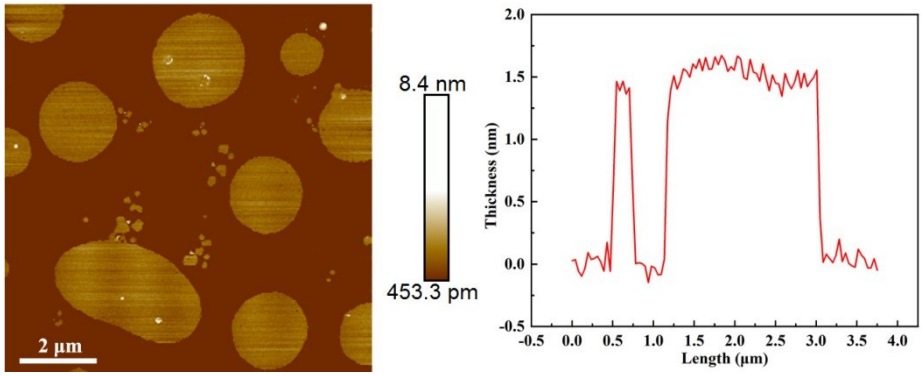

Figure S6. AFM results of CC/MoS_2@RGO-700 textile.

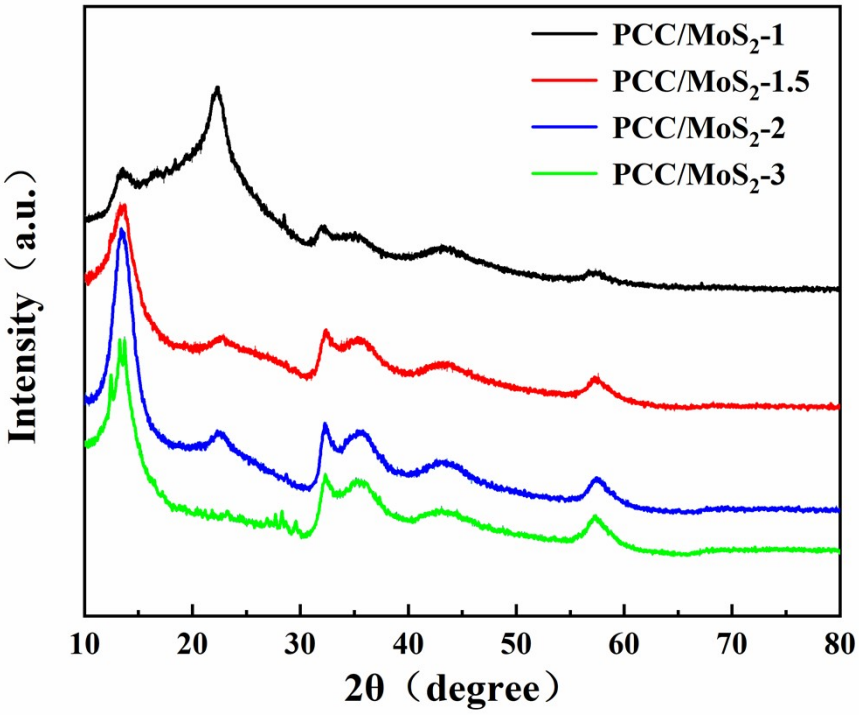

Figure S7. XRD patterns of PCC/MoS_2 samples.

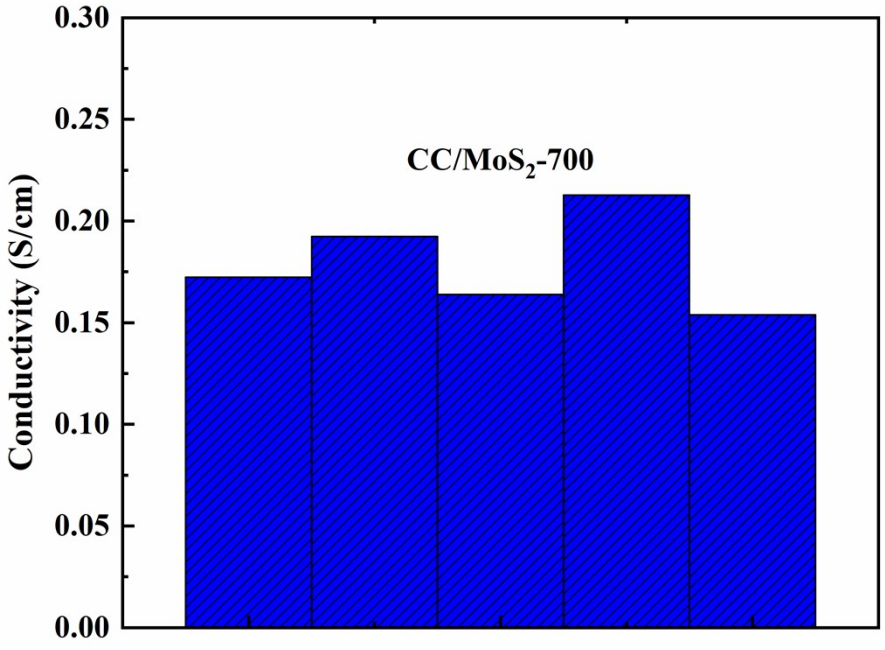

Figure S8. Electric conductivity of CC/MoS_2-700.

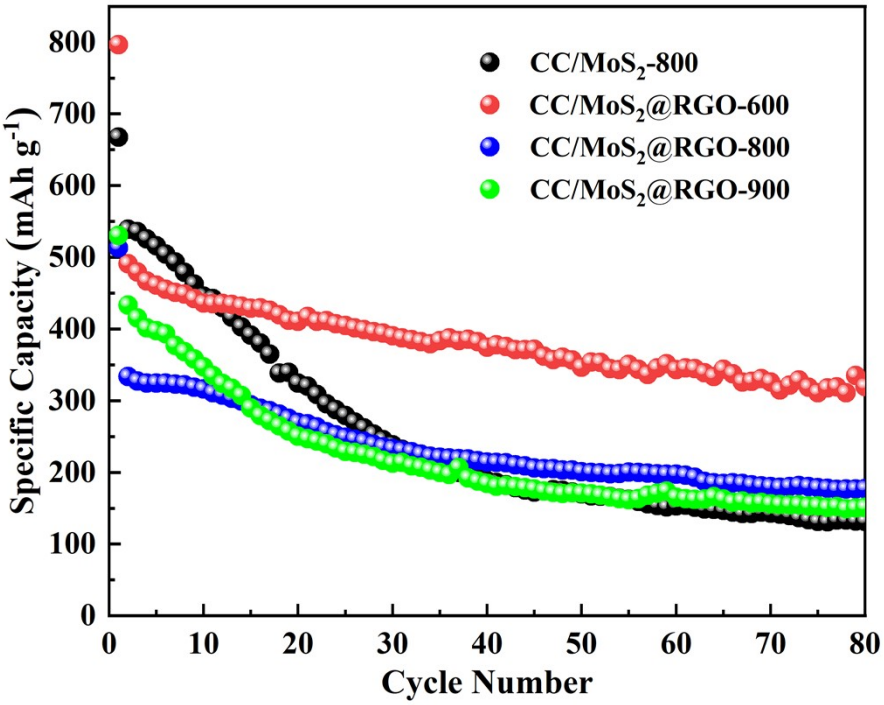

Figure S9. Cycling performances of CC/MoS_2-800, CC/MoS_2@RGO-600, CC/MoS_2@RGO-800 and CC/MoS_2@RGO-900 at 100 mA g^{-1}.

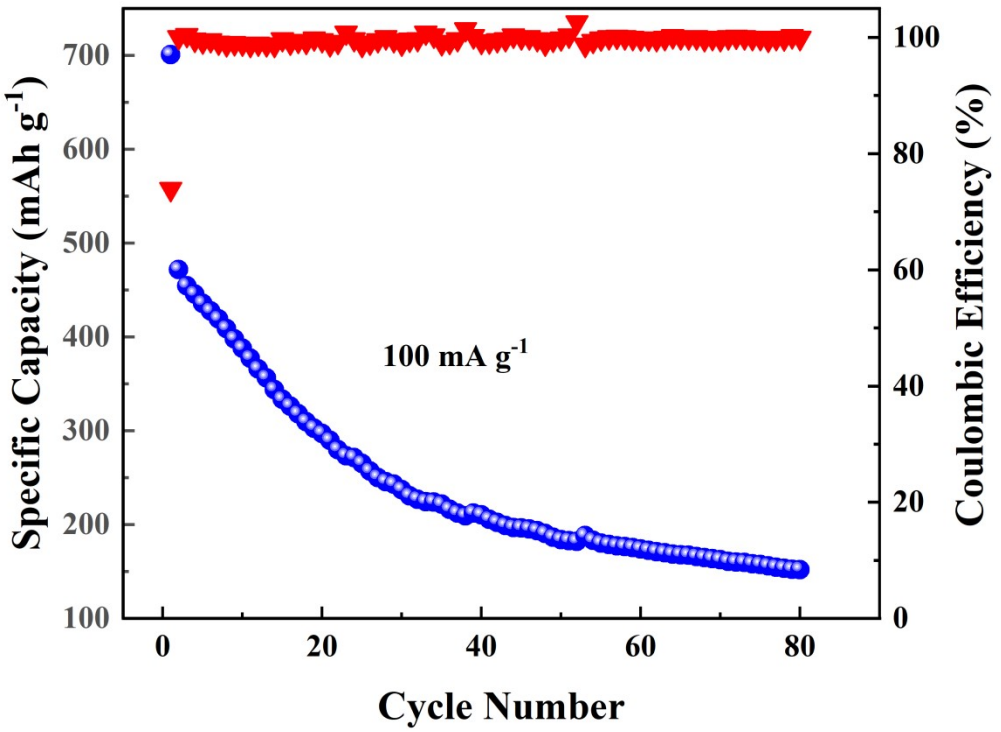

Figure S10. Cycling performance and CE profiles of PCC/MoS_2-900 at 100 mA g^{-1}.

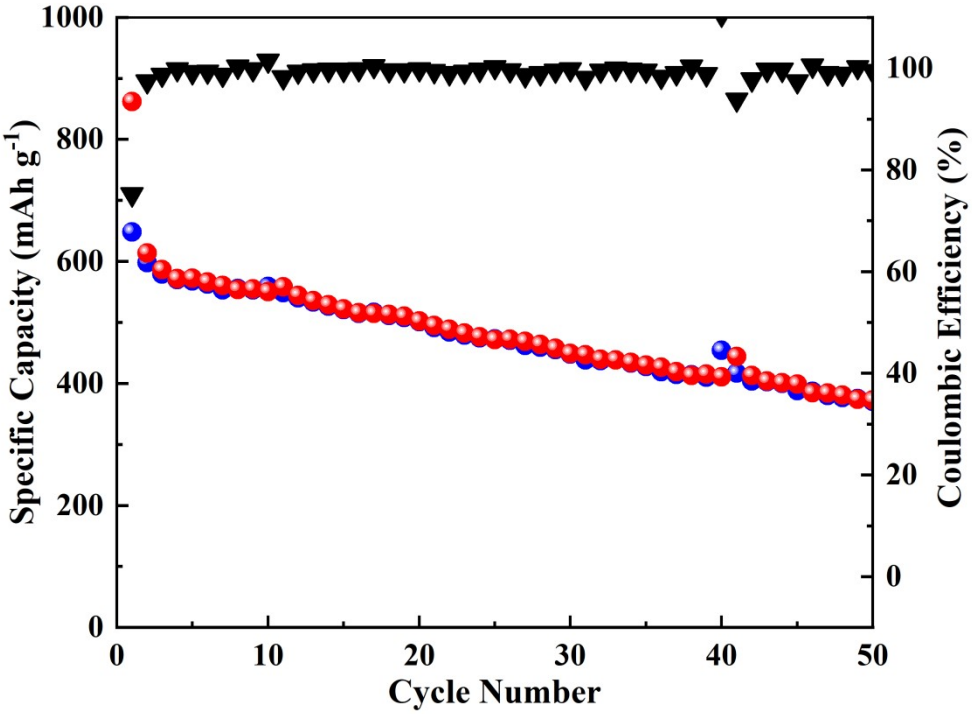

Figure S11. Cycling performance of CC/MoS_2@RGO-700 electrode at 50 mA g^{-1} for SIBs.

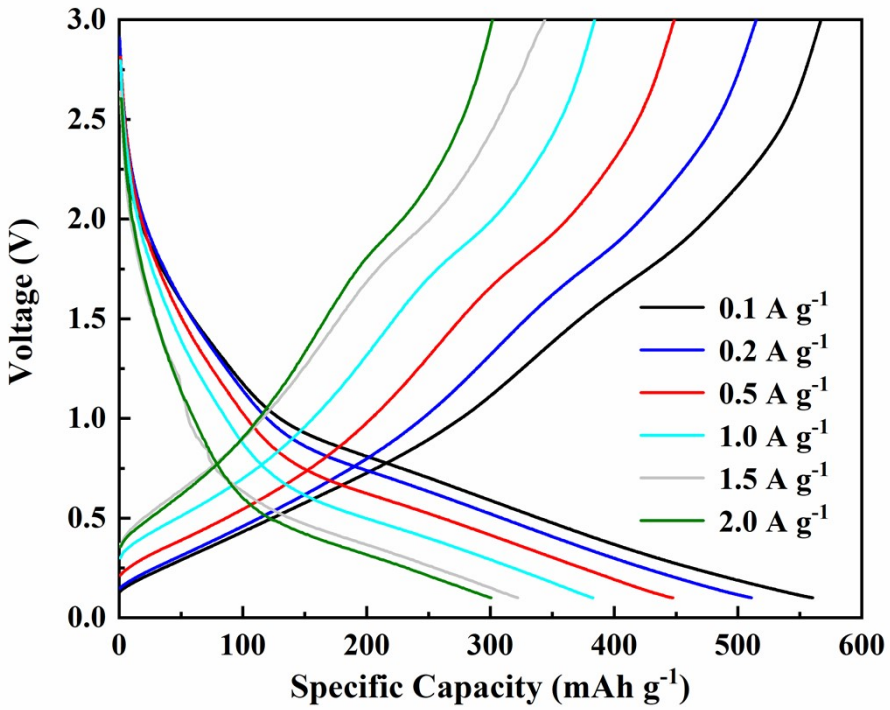

Figure S12. Discharge/charge profiles of CC/MoS_2@RGO-700 at various current densities in Na half cells.

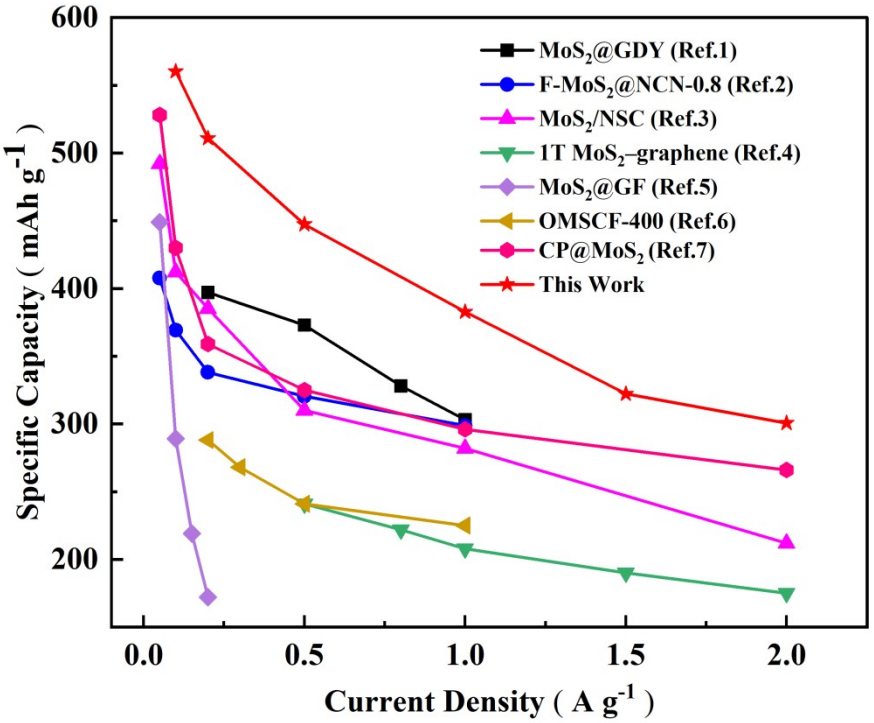

Figure S13. Comparison of rate capabilities for the MoS_2-based materials.

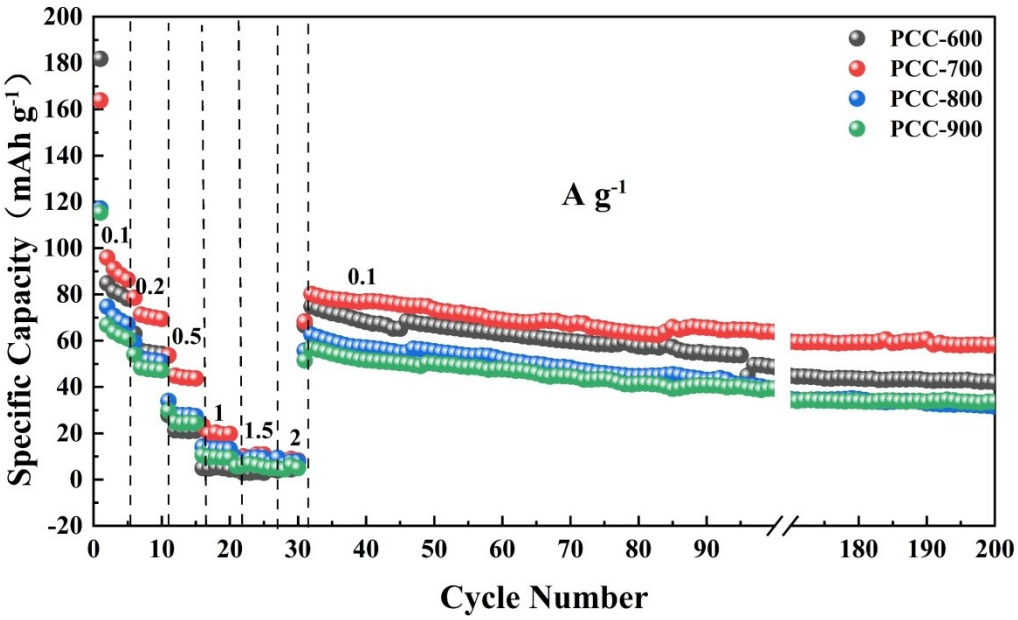

Figure S14. Rate capabilities of PCC at various current densities for sodium storage.

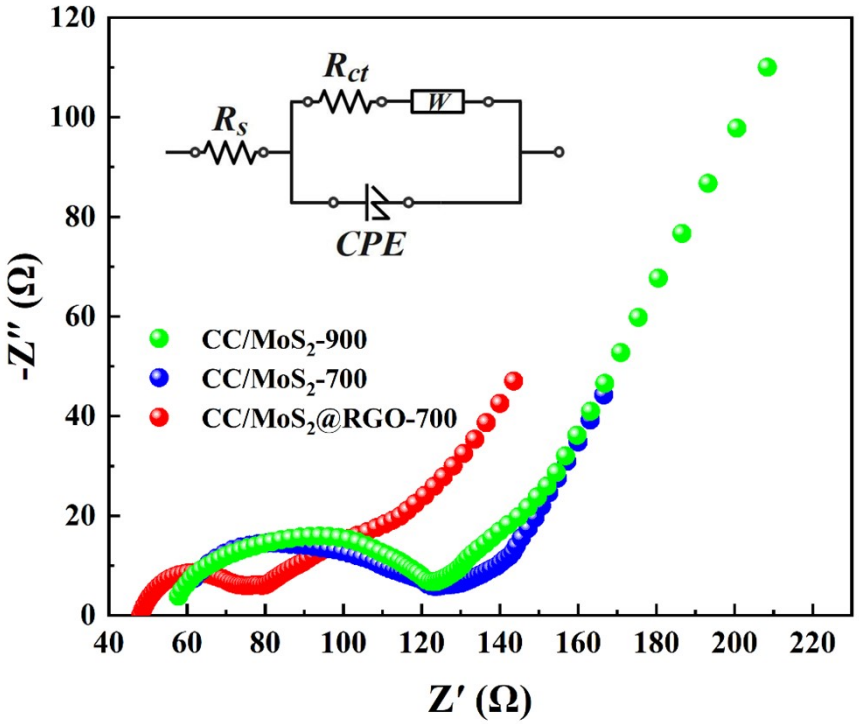

Figure S15. EIS curves of CC/MoS_2-700, CC/MoS_2-900 and CC/MoS_2@RGO-700 electrodes in Na half cells after 10 cycles, and the inset is the equivalent circuit.

Table S1. Comparison of R_{ct} values in Na half cells after 5 and 10 cycles.

Cycle	CC/MoS_2-700	CC/MoS_2-900	CC/MoS_2@RGO-700
5th	37.74 Ω	25.61 Ω	30.24 Ω
10th	68.72 Ω	67.26 Ω	36.53 Ω

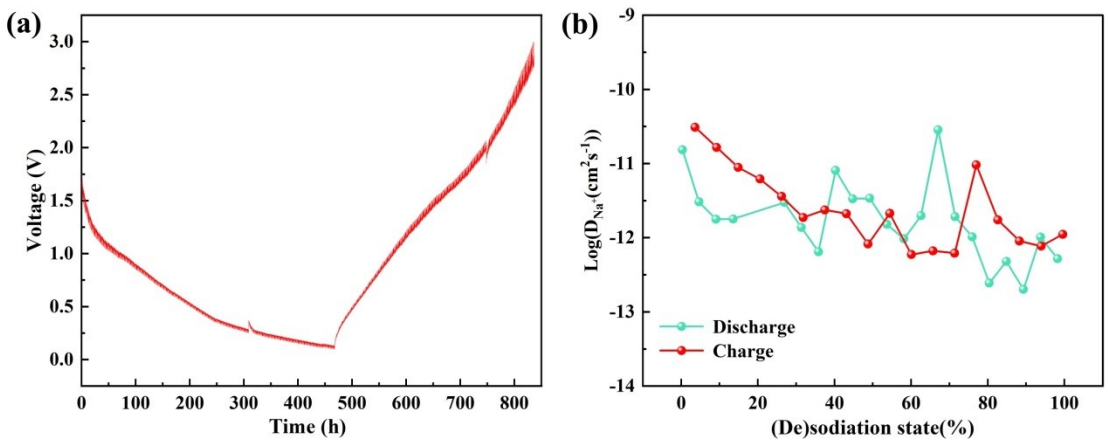

Figure S16. GITT curve and Na^+ diffusion coefficient for CC/MoS_2@RGO-700 electrode.

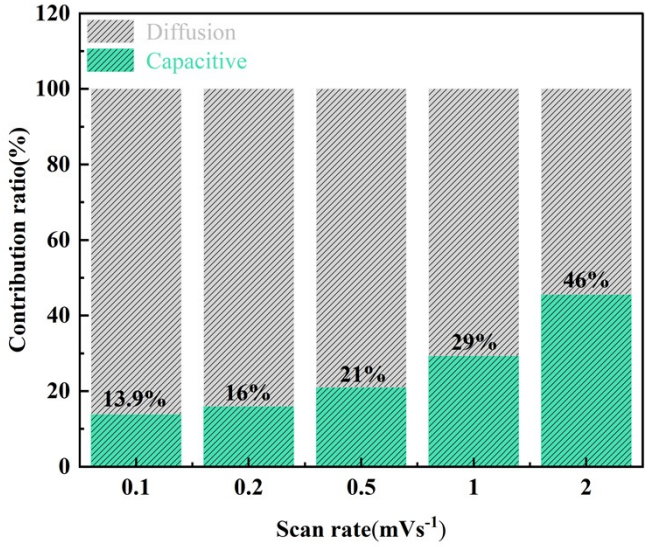

Figure S17. Contribution ratio of capacitive and diffusion-controlled capacities in Na half cells at various scan rates of CC/MoS_2@RGO-700.

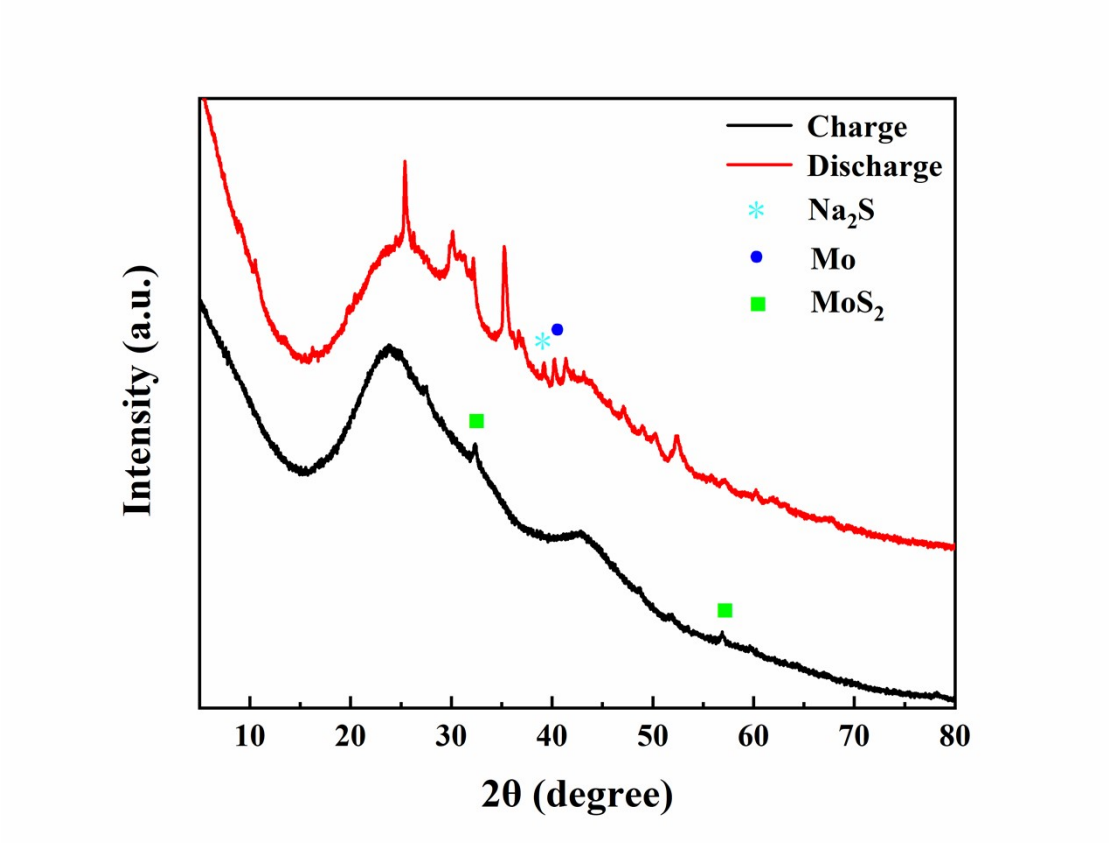

Figure S18. Ex situ XRD patterns of CC/MoS_2@RGO-700 electrode in Na half cells during the first cycle.

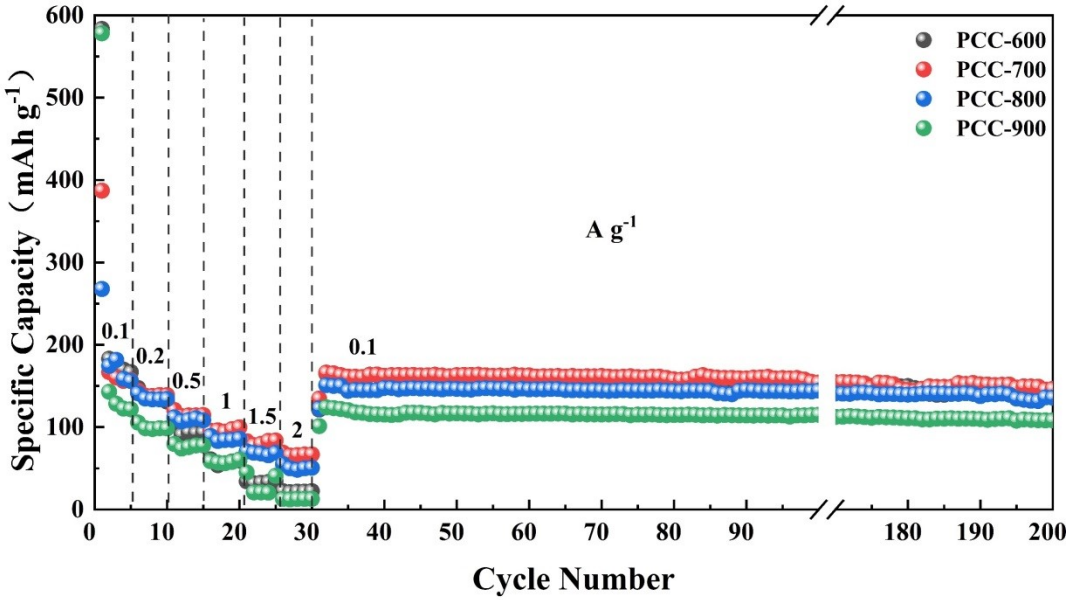

Figure S19. Rate capabilities of PCC at various current densities for lithium storage.

Table S2. Rate capabilities of PCC for lithium storage.

Material	Capacity (mAh/g)					
	0.1 A/g	0.2 A/g	0.5 A/g	1 A/g	1.5 A/g	2 A/g
PCC-600	174.5	136	93.2	56.1	32.5	21.7
PCC-700	160.3	137.8	114.2	94.2	79.6	66.1
PCC-800	181.6	133.6	108.6	84.2	67.9	48.3
PCC-900	128.4	97.6	75.7	56.1	20.8	12.8

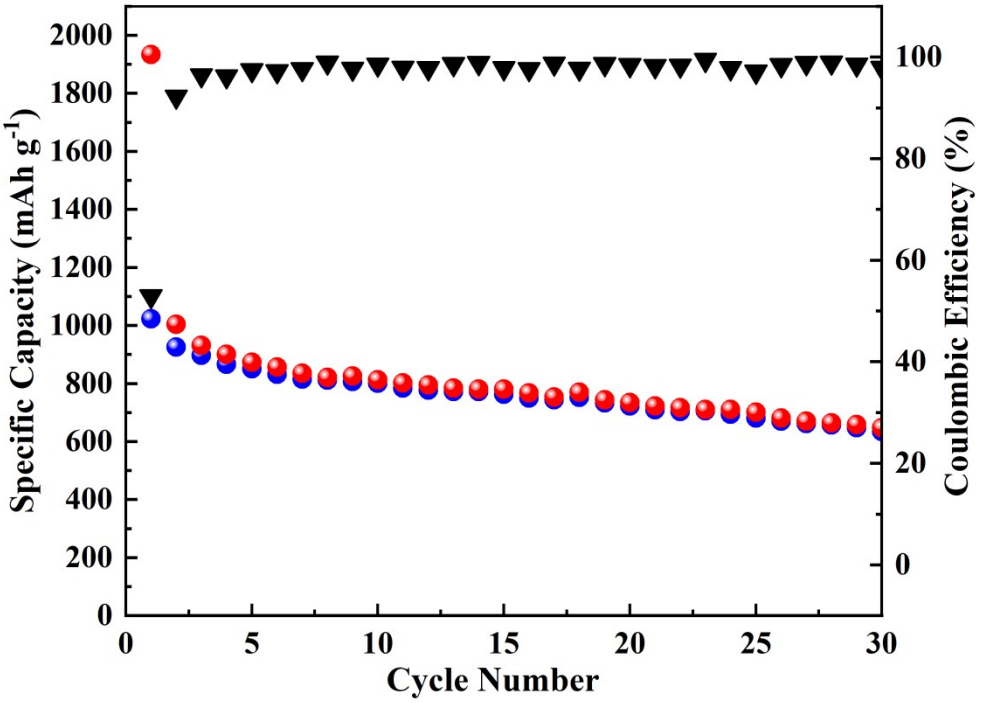

Figure S20. Cycling performance of CC/MoS_2@RGO-700 electrode at 50 mA g^{-1} for LIBs.

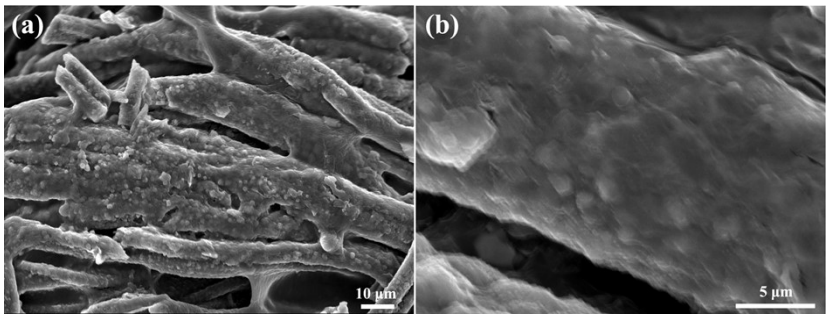

Figure S21. Morphology characterization of CC/MoS_2@RGO-700 electrode after cycling.

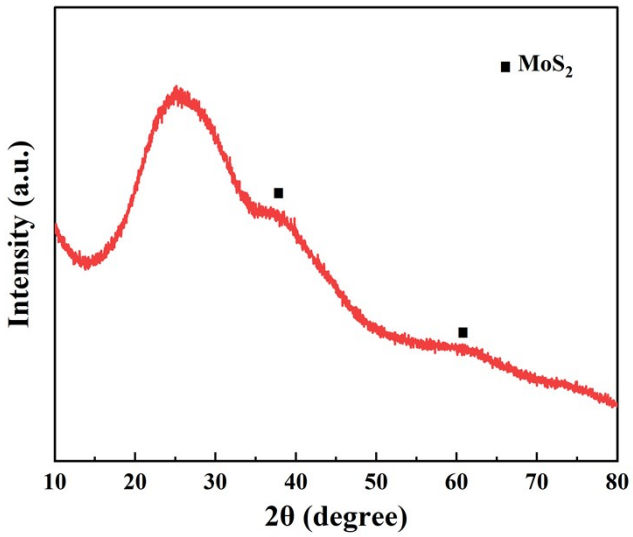

Figure S22. Structural characterization of CC/MoS_2@RGO-700 electrode after cycling.

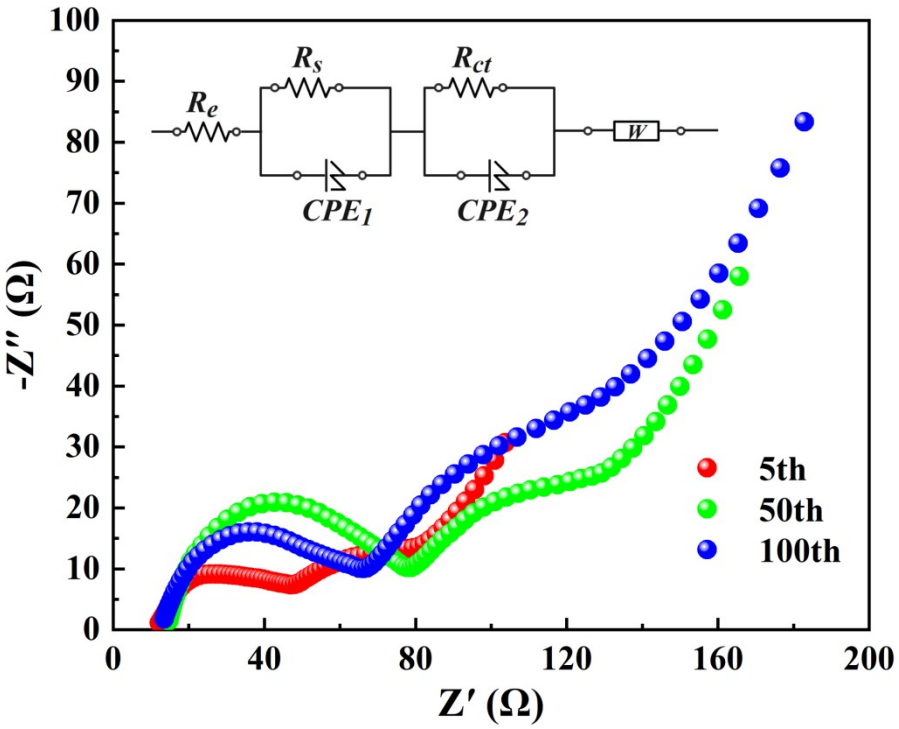

Figure S23. Nyquist plots of CC/MoS_2@RGO-700 electrodes in Li half cells after different cycles, and the equivalent circuit used for analysis.

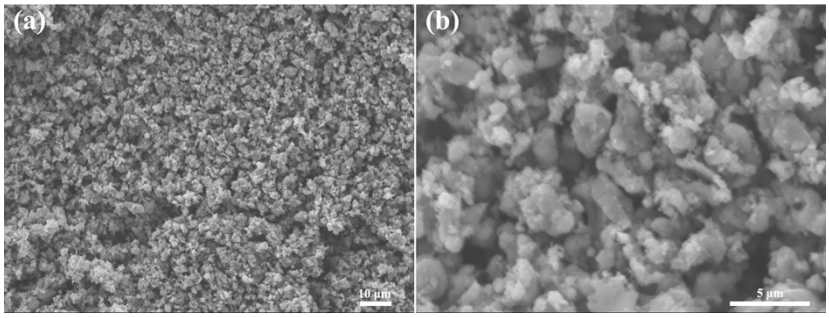

Figure S24. SEM images of $LiFePO_4$.

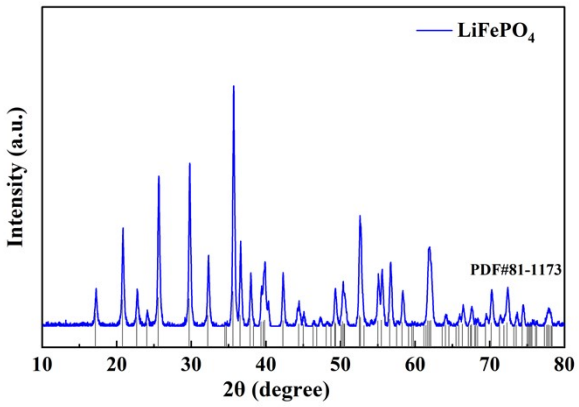

Figure S25. XRD pattern of $LiFePO_4$.

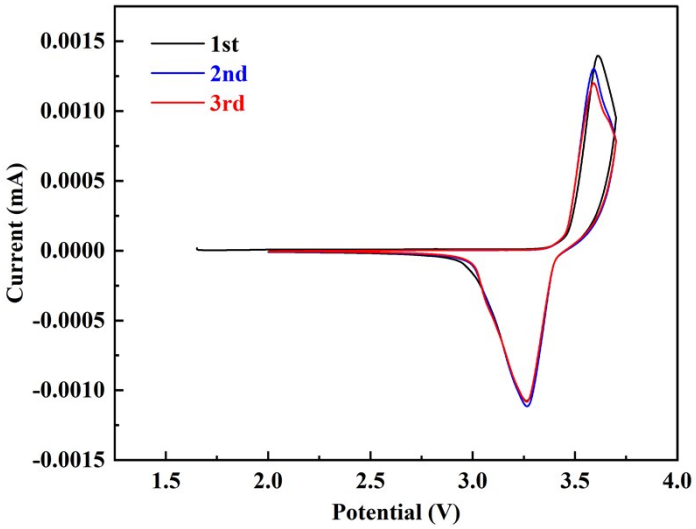

Figure S26. CV curves of $LiFePO_4$ electrode at 0.1 mV s^{-1}.

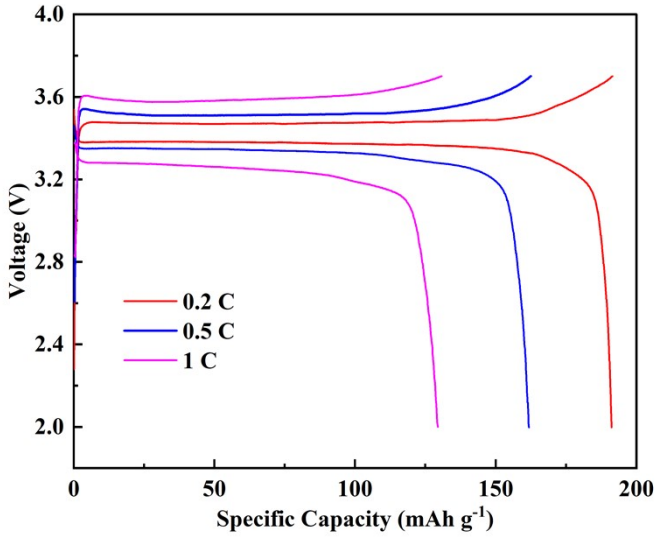

Figure S27. Charge/discharge profiles of $LiFePO_4$ electrode at different rates.

Supporting References

[1] Xu, J.; Liu, Q.; Dong Z.; Wang, L.; Xie, X.; Jiang, Y.; Wei, Z.; Gao, Y.; Zhang, Y.; Huang, K. Interconnected MoS_2 on 2D graphdiyne for reversible sodium storage. *ACS Appl. Mater. Interfaces* 2021, *13*, 54974-54980.

[2] Li, J.; Gao, W.; Huang, L.; Jiang, Y.; Chang, X.; Sun, S.; Pan, L. In situ formation of few-layered MoS_2@N-doped carbon network as high performance anode materials for sodium-ion batteries. *Appl. Surf. Sci*. 2022, *571*, 151307.

[3] Wang, T.; Xi, Q.; Wang, K.; Zeng, Z.; Du, Z.; Xu, Z.; Xie, L.; Ai, W.; Huang, W. Covalently binding ultrafine MoS_2 particles to N, S co-doped carbon renders excellent Na storage performances. *Carbon* 2021, *184*, 177-185.

[4] Geng, X.; Jiao, Y.; Han, Y.; Mukhopadhyay, A.; Yang, L.; Zhu, H. Freestanding metallic 1T MoS_2 with dual ion diffusion paths as high rate anode for sodium-ion batteries. *Adv. Funct. Mater.* 2017, *27(40)*, 1702998.

[5] Xiang, J.; Dong, D.; Wen, F.; Zhao, J.; Zhang, X.; Wang, L.; Liu, Z. Microwave synthesized self-standing electrode of MoS_2 nanosheets assembled on graphene

foam for high-performance Li-Ion and Na-Ion batteries. *J. Alloys Compd*. 2016, *660*, 11-16.

[6] Zhang, Y.; Tao, H.; Li, T.; Du, S.; Li, J.; Zhang, Y.; Yang, X. Vertically oxygen-incorporated MoS_2 nanosheets coated on carbon fibers for sodium-ion batteries. *ACS Appl. Mater. Interfaces* 2018, *10*, 35206-35215.

[7] Tu, F.; Han, Y.; Du, Y.; Ge, X.; Weng, W.; Zhou, X.; Bao, J. Hierarchical nanospheres constructed by ultrathin MoS_2 nanosheets braced on nitrogen-doped carbon polyhedra for efficient lithium and sodium storage. *ACS Appl. Mater. Interfaces* 2019, *11*, 2112-2119.